Engineering Structures 303 (2024) 117494

Contents lists available at ScienceDirect

Engineering Structures

journal homepage: www.elsevier.com/locate/engstruct

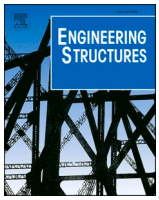

# Numerical analysis of potential failure modes in shear walls of the tunnel form concrete system: Performance-based approach

Vahid Mohsenian [a,1], Luigi Di-Sarno [b,*,2]

[a] Department of Civil Engineering, University of Science and Culture, Tehran, Iran
[b] Department of Civil and Environmental Engineering, University of Liverpool, Liverpool, UK

ARTICLE INFO

*Keywords:*
Tunnel-form concrete system
Reinforced concrete wall failure mode
Deformation-control action
Force-control action
Energy dissipation

ABSTRACT

Similar to other structural systems, the nonlinear modeling process of the tunnel-form concrete system necessitates an understanding of the potential failure modes in its primary lateral load-bearing members. With the identification of failure modes in the elements, deformation-control actions, force-control actions and deformation parameters are determined, making the analysis/design process straightforward. Given the unique characteristics of the tunnel-form concrete system, the applicability of design requirements and assumptions proposed for other similar systems for this structural system remains uncertain. In this study, to assess the potential failure modes of the walls of the system, two different modeling scenarios were utilized, employing pushover and time-history analyses. Within the scope of the studied 5- and 10-story buildings and the adopted assumptions, the results revealed that in the walls, shear is controlled by deformation and bending is force-control. In the incremental analysis, the bending failure mode of the walls (reaching yielding in vertical rebars) was estimated to be almost 10% higher than that of the shear failure mode (achieving an immediate occupancy limit). In the time-history analysis, under the design hazard level (475-year return period), the shear strain in the walls exceeded 13 times the strain at the onset of nonlinear shear behavior. This is because the wall sections still retained sufficient flexural-axial capacity and, contrary to code-based predictions, remained far from the flexural failure mode. The investigations further demonstrated that shear failure in the system was sufficiently ductile and capable of adequately absorbing and dissipating seismic input energy.

## 1. Introduction

The notable capability of simultaneously providing significant stiffness and lateral resistance has transformed tunnel-form concrete systems into a reliable lateral load resisting system [1]. According to analytical studies, the high capacity of the system is justifiable not only for strong earthquakes but also for substantial aftershocks [2]. Recent earthquakes have validated this claim. Following the earthquakes in Turkey in 1999, investigations have demonstrated that concrete tunnel-form system exhibit superior performance compared to conventional reinforced concrete systems [3]. Similarly, assessments carried out after the earthquakes and aftershocks of 2023 in Turkey have yielded similar results. Through field inspections conducted in earthquake-affected regions, no collapses were observed in concrete tunnel-form buildings, and the system endured minimal damage (see Fig. 1 as an example). However, considering the ability of the shear wall to prevent extensive damage and the prevalence of these elements within the tunnel-form system, these observations are not unexpected [4].

In studies performed by Balkaya and Kalkan [3,5], the three-dimensional behavior of the tunnel-form system was demonstrated. In these studies, the tensile-compressive behavior of the intersecting wall assembly was identified as a critical factor in providing the lateral load-bearing capacity of the system.

According to the study performed by Yuksel and Kalkan [6], the failure modes in a tunnel-form system can be brittle. In these studies, adding concentrated rebars at the wall corners has been reported as a desirable factor for avoiding brittle failure modes [7].

In experimental study conducted by Brunesi et al. [8], the connection of beams to walls in a tunnel-form system was investigated. In this study,

* Corresponding author.
*E-mail addresses:* v.mohsenian@usc.ac.ir (V. Mohsenian), luigi.di-sarno@liverpool.ac.uk (L. Di-Sarno).
[1] ORCID Number: 0000-0002-5918-1569
[2] ORCID Number: 0000-0001-6244-3251

https://doi.org/10.1016/j.engstruct.2024.117494
Received 16 September 2023; Received in revised form 24 November 2023; Accepted 5 January 2024

**Fig. 1.** Intact Concrete Tunnel-Form Buildings after Experiencing Strong Earthquakes and Aftershocks (Turkey, 2023).

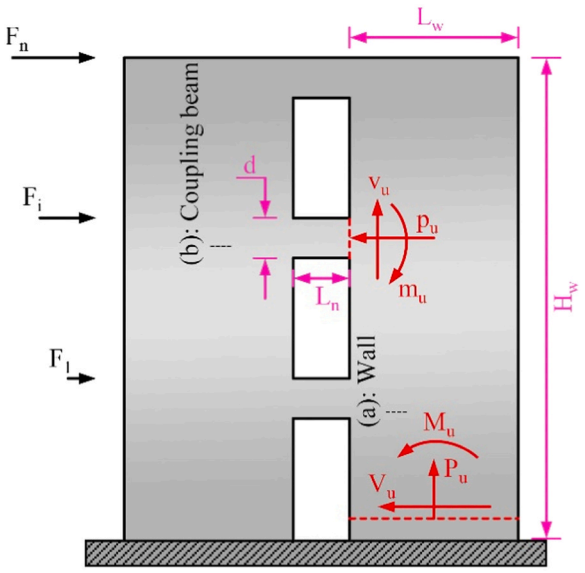


**Fig. 2.** Internal forces resulting from lateral loading (a)-Shear walls (b)-Coupling beams.

cracking was observed in the wall-to-foundation connection during the cyclic loading of a laboratory-scale model, as well as cracking at the connection point of the beams to the walls. Similar results were also observed in the experimental part of the study by Tavafoghi and Eshghi [9].

Based on the existing technical literature and seismic studies, the failure modes in the tunnel-form system can be brittle and unexpected. Studies related to the assessment of the failure modes in systems are mostly limited to scaled laboratory models. Nevertheless, the possibility of utilizing and generalizing the results of such studies for multi-story models at real scales remains a question [10,11]. Unfortunately, there is no comprehensive code for the analysis and design of a concrete tunnel-form system. Based on the existing prescriptive design requirements, the system is currently categorized as a subset of "load-bearing wall" systems [12]. However, the acceptance of using seismic regulations and parameters of the "load-bearing wall" system for tunnel-form systems remains uncertain. The development of an independent seismic code for this system requires field studies and further research is still necessary.

Based on the provided explanations and existing challenges, the main research questions are as follows:

1. What are the deformation-control and force-control mechanisms in the primary lateral load-bearing members of the tunnel-form system (specifically, walls and wall components in this study)?
2. During performance-based analysis/design, what are the deformation parameters and the desired acceptance criteria for these elements?
3. In the dominant failure mode, what is the extent of energy absorption and dissipation within the system?
4. Does the existing categorization of the seismic behavior of shear walls also apply effectively to tunnel-form system?

This study aimed to answer these questions, and its hierarchy is presented in seven distinct sections. Section 2 presents the adopted methodology, and process of this study. Section 3 provides detailed descriptions of the studied models and the initial design of the structures. Section 4 elucidates the nonlinear modeling process and the adopted scenarios. Section 5 pertains to the structural analysis, employing modal pushover and time-history analyses. In this section, along with the derivation of the responses, the interpretation of the observations is presented. Section 6 is focused on energy considerations, and investigates the potential energy input and consumption for the probable failure mode within the system at the design hazard level. Finally, in Section 7, the key findings of this study are presented in detail.

## 2. Methodology

In a numerical study, evaluating the performance level of a tunnel-form concrete system requires the use of a precise computational model that can adequately capture the seismic behavior and potential failure mechanism of the members. An analytical model of a shear wall (or wall components) is only considered desirable when its stiffness (flexural, shear, and axial), strength, and deformation capacity are close to reality.

Based on the type of element failure, its behavior is classified as deformation-control or force-control, each of which has its own modeling process and acceptance criteria. Deformation-control behavior is ductile and energy dissipative, whereas force-control behavior is brittle; during this mode, the element fails without significant energy dissipation. In a deformation-control element, each of the internal actions (including flexural moment ($M_u$), shear force ($V_u$), and axial force ($P_u$)) will lead to different failure modes based on the level and potential for nonlinear behavior (Fig. 2). In shear walls and wall components, deformation control behavior is limited to flexural moment ($M_u$) and shear force ($V_u$) [13]. In the following, the important modeling parameters and acceptance criteria for each case are elaborated.

### 2.1. Elements with dominant flexural behavior

Under lateral loading, if the nonlinear behavior of the wall is due to flexural actions, the nonlinear deformation parameter is the rotation at the top of the plastic region located at the end of the wall (see parameter $\theta_1$ in Fig. 3(a)) [14]. For coupling beams, the rotation value at the plastic hinge location is considered the deformation parameter of interest (see parameter $\theta_2$ in Fig. 3(b)). Such elements are susceptible to forming plastic hinges in flexural regions; therefore, the expected flexural strength of the member ($M_{CE}$) is utilized in the modeling process. The expected strength of the elements ($Q_{CE}$) is calculated using available computational methods, disregarding any reduction factors (partial safety factors are set to 1). In the corresponding calculations, it is

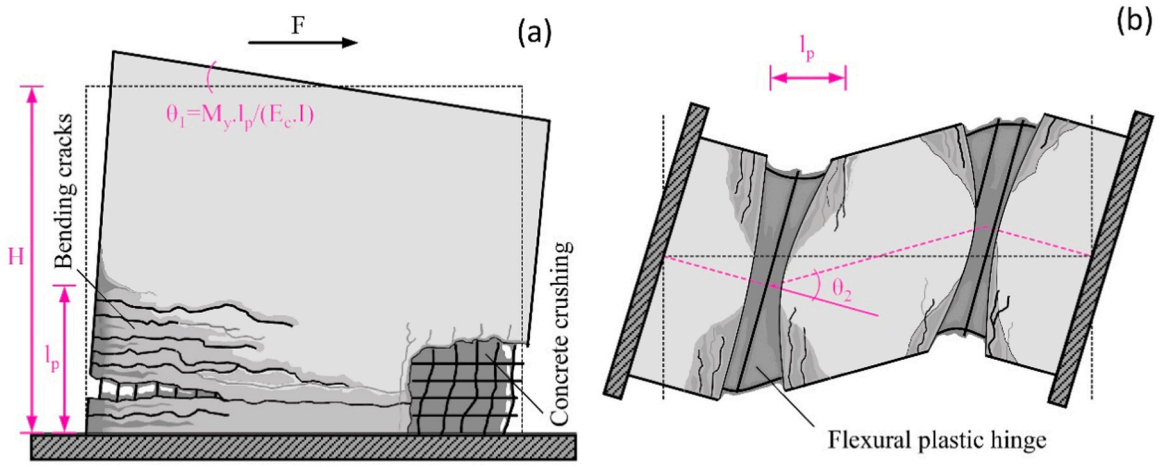


**Fig. 3.** Nonlinear deformation due to flexural failure and corresponding response parameter in (a) Shear walls (b) Coupling beams.

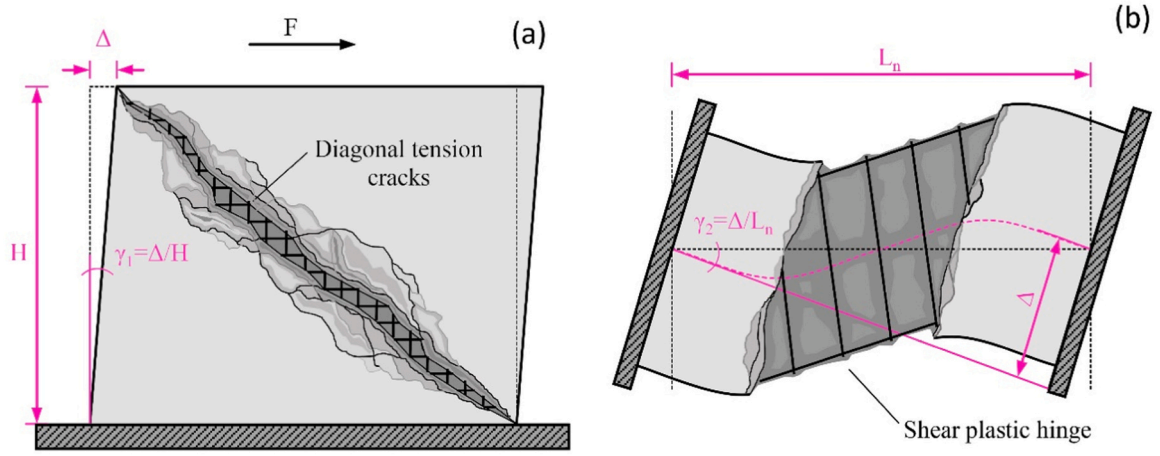


**Fig. 4.** Nonlinear deformation due to shear failure and corresponding response parameter in (a) Shear walls (b) Coupling beams.

implicit that the expected strengths of the materials will be used [13]. In Fig. 3, parameter ($l_p$) denotes the length of the plastic zone. In the seismic analysis, the deformation requirement of each member ($\theta_u$) was considered as the response. A comparison of the extracted values with the critical values, such as different performance levels ($\theta_{IO}$, $\theta_{LS}$ and $\theta_{CP}$), determines the local performance level of the member. Obviously the values of the limit states for different performance levels (including $\theta_{IO}$, $\theta_{LS}$ and $\theta_{CP}$) are taken for ASCE (refer to Table 10–19 in ASCE) [13].

In this failure mode, shear ($V_u$) and axial force ($P_u$) actions are considered force-control, and the maximum demand of each action must inherently be lower than the lower bound of its corresponding strength ($V_u < V_{CL}$ and $P_u < P_{CL}$).

The lower bound of the member strength ($Q_{CL}$) was also calculated using available computational methods, disregarding any reduction factors. In this case, the lower bound of the material strength will be used in the related equations [13].

According to previous studies, geometric properties and section reinforcement conditions are important factors that influence the flexural failure modes of shear walls [15]. In the concrete structure design code [16], shear-flexural behavior is attributed to a wall when the parameter α, defined as the ratio of the wall height ($H_w$) to its length ($L_w$) ($\alpha = \frac{H_w}{L_w}$), is greater than 2 (see Fig. 2). ASCE introduces a critical value of three for this ratio [13].

### 2.2. Elements with dominant shear behavior

Under lateral loading, if the nonlinear behavior of the wall results from shear actions, the nonlinear deformation parameter is the shear strain (relative lateral displacement) of the wall (see parameter $\gamma_1$ in Fig. 4(a)) [14]. For coupling beams, chord rotation is the measure (see parameter $\gamma_2$ in Fig. 4(b)).

Such elements are susceptible to forming plastic shear hinges, and it is evident that the expected shear strength of the member ($V_{CE}$) is utilized in the modeling process. During the structural analysis, comparing the deformation demand of each member ($\gamma_u$) with critical values, i.e., different performance levels ($\gamma_{IO}$, $\gamma_{LS}$ and $\gamma_{CP}$), determines the local performance level of the member. In this case, numerical values corresponding to different performance levels in members (including $\gamma_{IO}$, $\gamma_{LS}$ and $\gamma_{CP}$) will be extracted from ASCE (refer to Table 10–20 in ASCE) [13].

In this circumstance, the flexural and axial force actions ($M_u$ and $P_u$, respectively) are force-controlled. Accordingly, the maximum demand for each action must be lower than the lower bound of its corresponding strength ($M_u < M_{CL}$ and $P_u < P_{CL}$). In this case, the expected and lower bound strengths of the elements ($Q_{CE}$ and $Q_{CL}$) are determined using valid computational methods and previous assumptions [13].

In the concrete structure design code [16], a shear-controlled and brittle behavior is attributed to a wall when the parameter α is less than 2. ASCE introduces a critical value of 1.5 for this ratio [13].

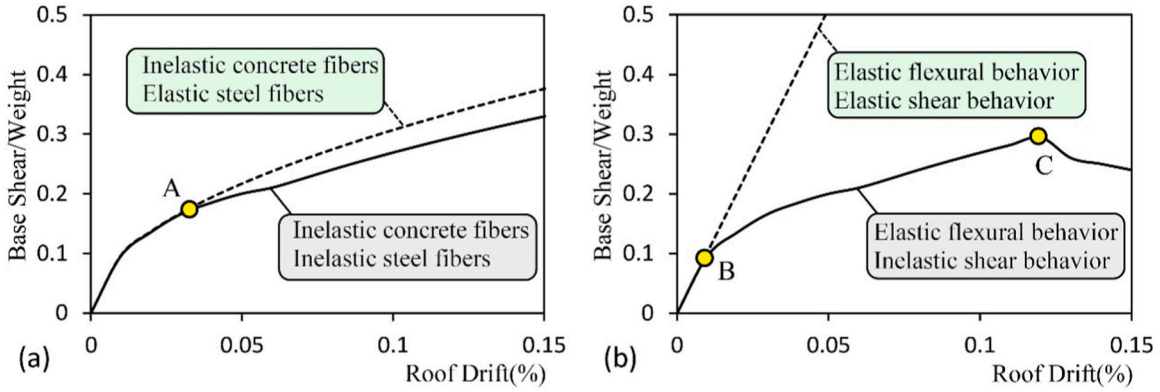


**Fig. 5.** Incremental analysis of a hypothetical fiber model and comparison of results (a) Linear shear behavior and nonlinear flexural behavior (b) Linear flexural behavior and nonlinear shear behavior.

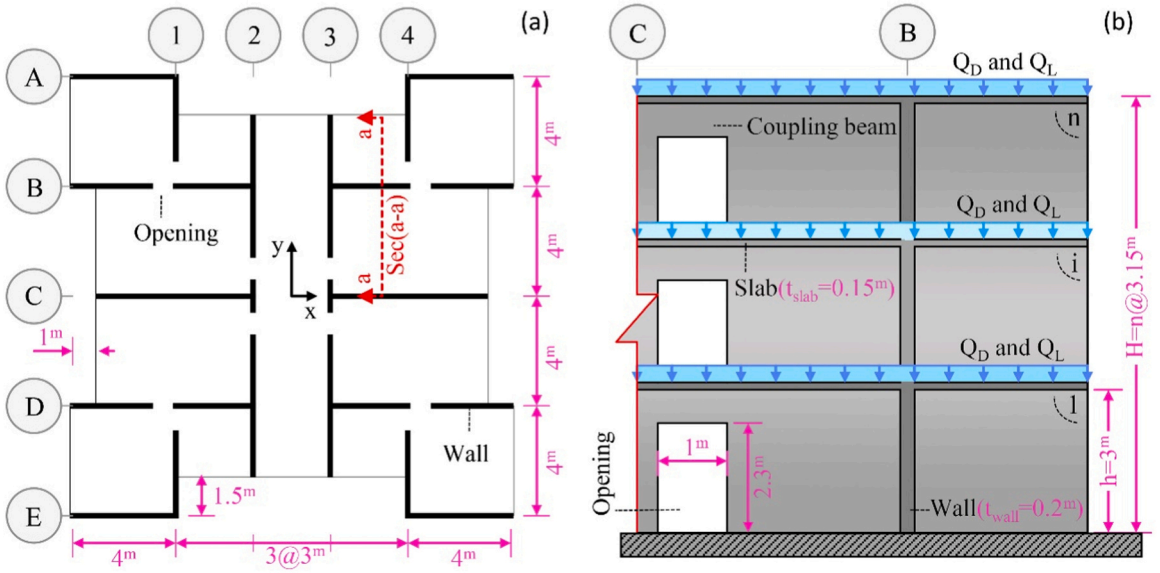


**Fig. 6.** Studied Tunnel-Form Buildings (a) Typical story plan (b) Elevation of the vertical section a-a in a hypothetical n-story model.

### *2.3. Considered approach to estimate the dominant behavior of elements*

Considering the explanations provided in subsections 2.1 and 2.2, depending on the anticipated failure mode of the elements, the process of performance analysis in terms of modeling and required controls is entirely different. Thus, the successful creation of a nonlinear model requires an understanding of the governing behavior of the elements.

Flexural failure of walls undoubtedly involves the yielding of their vertical reinforcements. In the modeling process using the distributed plasticity theory (fiber elements), by accounting for the linear shear behavior of the elements, the time of yielding of vertical flexural reinforcements can be easily determined. According to the hypothetical Fig. 5(a), comparing the results of incremental analysis of models that differ only in the assumed behavior curve of reinforcing bars, identifies the point of yielding of the vertical reinforcements (point A).

In the same model, whenever the flexural behavior of the elements is linear and their shear behavior is nonlinear, as depicted in the hypothetical Fig. 5(b), comparing the results of incremental load analysis identifies points corresponding to shear failures (points B and C). Now, comparing the base shear with the points mentioned provides a desired insight for judging the probable failure mode.

In the current study, to identify the dominant failure mode in the tunnel-form concrete system, the described scenario has been utilized. Ultimately, to validate the predicted failure mode, the acceptance criteria of the elements (see explanations in Sections 2–1 and 2–2), as well as their energy absorption and dissipation capabilities, have been studied based on the results of time history analyses of the models.

## 3. Introduction of studied structures

This study is conducted on 5 and 10-story tunnel-form buildings (n = 5 and 10) with story plans as shown in Fig. 6(a). It is noted that the selected story plan is geometrically regular and symmetric with respect to its main axes (x and y). As shown in Fig. 6(b), the net height of the stories is 3 m. For dead and live loads on the stories ($Q_D$ and $Q_L$), uniform distribution with intensities of 6.4 and 2 kN/m$^2$, respectively, have been considered (the roof live load is 1.5 kN/m$^2$).

It is assumed that the buildings have a medium importance level and are constructed in a site with high seismic potential (475-year return period and a maximum considered ground motion of 0.35 g) with a stiff foundation (site class C according to ASCE classification [17]) and shear wave velocity ranging from 357 to 750 m/s. The studied buildings have been designed according to the Iranian Seismic Code (Standard 2800) [18] and the American Concrete Code [16], using the software ETABS [19].

In the design process, the thicknesses of the slabs and walls have been

**Table 1**
Modal parameters of structures including the vibration periods (T) and the mass participation factors (M).

| Mode no. | Situation | 5-storey building | | 10-storey building | |
|---|---|---|---|---|---|
| | | T (s) | M (%) | T (s) | M (%) |
| 1 | Torsional | 0.223 | 0.00 | 0.748 | 0.00 |
| 2 | Translational in y-diraction | 0.139 | 79.60 | 0.445 | 75.41 |
| 3 | Translational in x-diraction | 0.134 | 74.02 | 0.318 | 67.35 |
| 4 | Torsional | 0.052 | 0.00 | 0.148 | 0.00 |
| 5 | Translational in x-diraction | 0.041 | 19.51 | 0.096 | 20.87 |
| 6 | Translational in y-diraction | 0.037 | 14.18 | 0.095 | 14.47 |

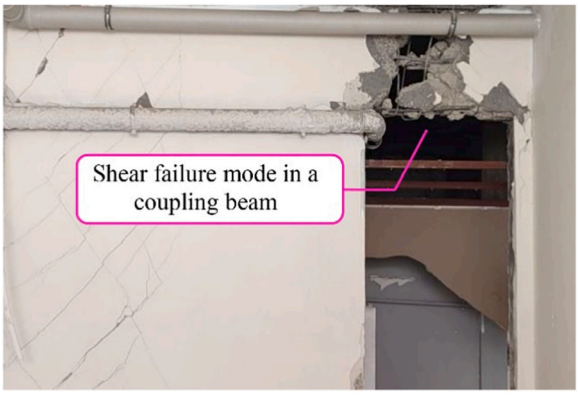


**Fig. 7.** Shear failure of a coupling beam in a Tunnel-Form Building (Turkey, 2023).

considered as 150 and 200 mm, respectively. The selection of these thicknesses ensures linear behavior for the slabs under seismic loads and provides a minimum relative plan area of 3% for the walls [12]. The yield strength of the rebars ($f_y$) and the characteristic compressive strength of the concrete ($f_c$) are taken as 400 and 25 MPa, respectively. The slabs are reinforced with two parallel layers of $\phi$8 rebars with a spacing of 250 mm. The walls are also reinforced with two parallel layers of $\phi$8 rebars with a spacing of 200 mm (except for the first four stories of the 10-story building, where $\phi$12vertical rebars are used). The length of the coupling beams above the openings is set to 1000 mm, and their section height is 700 mm (refer to Fig. 6).

The specifications of the first six vibration modes of the buildings are extracted according to Table 1. It is noteworthy that despite the regularity and symmetry in the models, the first mode is torsional. This phenomenon, which is common in tunnel-form concrete buildings, can be attributed to the reduced torsional stiffness resulting from the lower relative wall density in the internal areas of the plan [20]. In fact, the specific construction conditions of the tunnel form system and the necessity of removing the forms from the surrounding faces of the plan prevent the existence of structural walls in these sections. As expected, in both buildings, the dominant translational mode is related to the y-direction. This direction corresponds to the lower relative percentage of walls in the plan, and consequently, the lateral stiffness in this direction is lower. In the following, the y-axis was considered as the main plan axis.

It is observed that in the first vibrational mode in the analysis direction (y), the period is less than 1 s, and the effective mass ratio is over 75%. In this regard, assuming a triangular distribution of lateral loads proportional to the first mode is close to reality [13]. However, for the other direction (x) and especially in taller buildings, this assumption is not valid. The results show that considering the participation of higher modes is essential for analyzing the system.

## 4. Nonlinear modelling of elements

The nonlinear modeling and analysis of the structures have been performed using the PERFORM_3D software [21]. This software is tailored for performance-based analyses and fully complies with the ASCE guidelines [13]. For modeling the elements in the software, a 4-node "shear wall" element has been utilized.

In coupling beams, geometric specifications are among the influential factors on the type of nonlinear behavior and failure mode. According to studies, when the ratio of the free span length of the beam ($L_n$) to its section height (d) is less than 2 ($L_n/d \leq 2$), the failure in the coupling beam is certainly of the shear type [22,23]. The results from empirical studies conducted by Mosoarca also demonstrate that the failure mode of coupling beams verifies this conclusion [24]. Moreover, the accuracy of assumption has also been confirmed in the 2023 Turkey

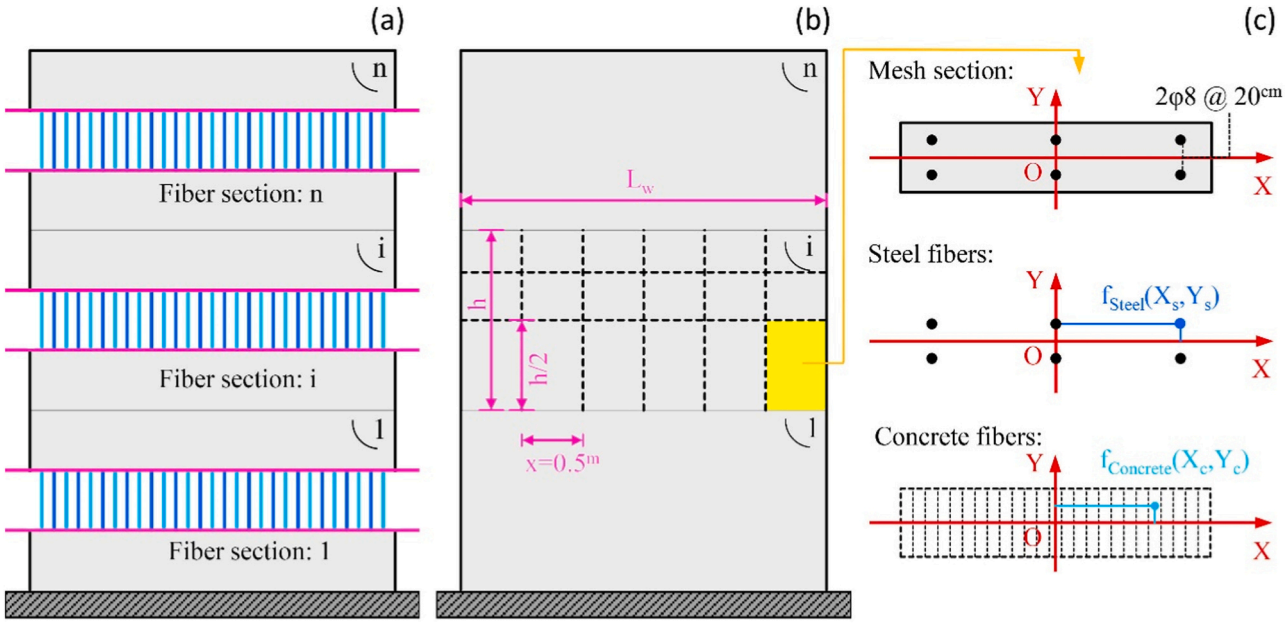


**Fig. 8.** Hypothetical shear wall of n stories using fiber elements (a) defined fibers along the height (b) discretization in the wall plane (c) Section discretization in a mesh plane.

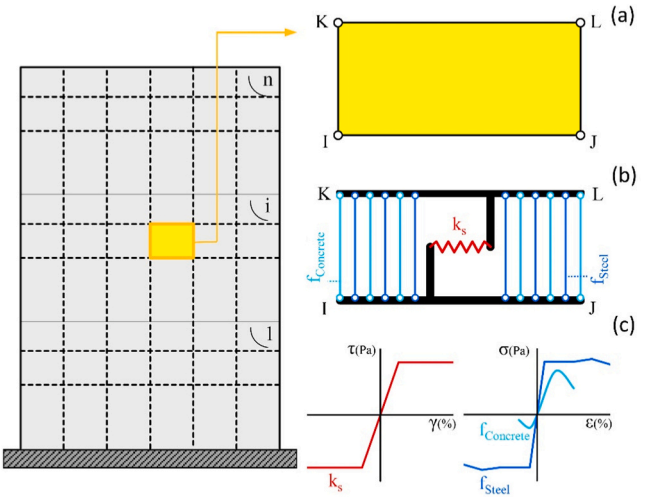


**Fig. 9.** Modeling a hypothetical n-story shear wall using a fiber model (a) 4-node shear wall mesh element (b) Considered behaviors for steel, concrete, and shear (c) Defined stress-strain behavior for fibers and shear spring.

earthquake (Fig. 7).

In the present study, the geometric specifications of the coupling beams ensure shear failure in them. Based on this, in the nonlinear behavior modeling of these elements, shear force is always considered as a deformation-control parameter.

The design of coupling beams is aimed at eliminating brittle and undesirable failure modes. To ensure ductile shear behavior, diagonal rebars, in addition to stirrups, have been considered for reinforcing these elements [22,23].

In the modeling process of cross-sections of shear walls using fiber elements, the conditions for the yielding of vertical rebars and the occurrence of flexural failures have been accounted for [25]. As shown in Fig. 8(a), by introducing nonlinear fibers throughout the height of the wall, the possibility of nonlinear behavior occurring in any part of it has been ensured. By considering the plastic hinge length ($l_p$) equal to half of the wall height [16], the fiber discretization of the walls in the vertical direction has been performed as depicted in Fig. 8(b). Due to the software limitations in specifying the number of fibers for a section (only 60 fibers), along the longitudinal direction, the walls have been discretized every 50 cm (refer to Fig. 8(b)).

In each mesh section located on the wall plane, for each rebar in its current position, a steel fiber has been defined. To define concrete fibers, the wall has been discretized into two fibers along its thickness, and along the length of the wall, a new fiber has been defined every 2 cm (see Fig. 8(c)). Now, each concrete fiber with an area of 20 $cm^2$ will be located the center of its mesh surface in the local coordinate system.

As shown in Fig. 9, in the fiber-based wall model, the behavior of each mesh is a function of the defined behavior curves for steel ($f_{Steel}$), concrete ($f_{Concrete}$), and shear fibers ($k_s$) [26]. It is obvious that the flexural and axial strength of the section are provided by steel and concrete fibers. Accordingly, stress-strain (σ-ε) curves have been introduced for them separately, considering the characteristics of the materials (see Fig. 9(c)). In this study, steel and concrete fibers have been modeled using bilinear models with kinematic and isotropic hardening [27,28].

For the shear spring ($k_s$), the behavior is defined as a function of in-plane shear stress-strain (τ-γ) (see Fig. 9(c) again). Further detailed explanations will be provided in subsequent sections.

To address the research questions, two different scenarios have been considered in the wall modeling process. Each scenario is explained in detail as follows:

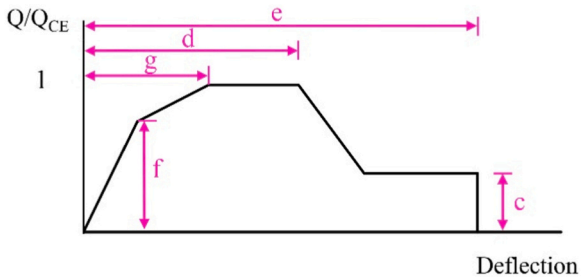


**Fig. 10.** Nonlinear shear behavior curve for shear-control elements [13].

### 4.1. Modelling based on assumption of nonlinear flexural and linear shear behavior

In the fiber-based model shown in Fig. 9, when the shear behavior of each mesh is linear, it is obvious that the nonlinear behavior of the structure will be solely a function of the behavior of steel and concrete fibers. In this modeling scenario, two different states are assumed for each structure. In the first state ($SM_1$), both steel and concrete fibers are nonlinear. In the second state ($SM_2$), the steel fiber behavior is linear while the concrete fiber is nonlinear. The difference in response between these two states is naturally attributed to the yielding of vertical reinforcing bars.

### 4.2. Modelling based on assumption of linear flexural and nonlinear shear behavior

In this modeling approach, as depicted in Fig. 9, the shear behavior is nonlinear while the flexural behavior is linear for each mesh. Linear behavior is assigned to the concrete and steel fibers ($f_{Steel}$ and $f_{Concrete}$). The flexural behavior of each mesh is assumed to be elastic. To model the nonlinear shear behavior in the elements ($k_s$), a force-deformation curve shown in Fig. 10 is utilized. This curve, referred to as the backbone cyclic behavior of the element, represents the expected shear capacity of the element for a given section ($Q_{CE} = V_{CE}$) and the values of parameters e, d, g, f, and c, are provided in ASCE standards [13].

In this scenario also two different states are considered for each structure. In the first state ($SV_1$), nonlinear shear behavior is considered. In the second state ($SV_2$), linear shear behavior is assumed. The difference in results between these two states arises from the elements entering the nonlinear behavior range under shear actions.

Rigid diaphragm, rigid connections, and neglecting foundation uplift as well as soil-structure interaction effects are among the other adopted assumptions in this study.

## 5. Structural analysis and system responses

The studied tunnel-form concrete buildings have been analyzed in the direction of the primary plan axis (y-axis). In the structural analysis process, the combination of gravity loads ($Q_G$) according to Eq.1 has been considered [13].

$$Q_G = Q_D + 0{\cdot}25Q_L \quad (1)$$

In this equation, $Q_D$ and $Q_L$ represent the dead and live load of the stories, respectively (Fig. 6).

As previously explained, determining the dominant behavior of the walls in the tunnel-form system has been carried out using pushover and time-history analyses. The process of each analysis and related assumptions are presented in the following subsections.

### 5.1. Pushover analysis

The pushover analysis has been conducted using the modal combination method. The pattern of applied lateral load in this method is

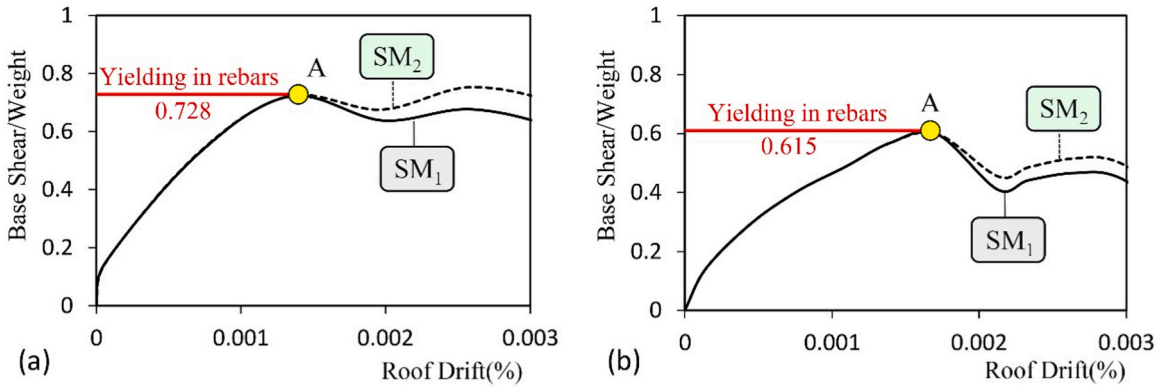


**Fig. 11.** Capacity curves of the models with linear shear and nonlinear flexural behavior (a) 5-story building (b) 10-story building.

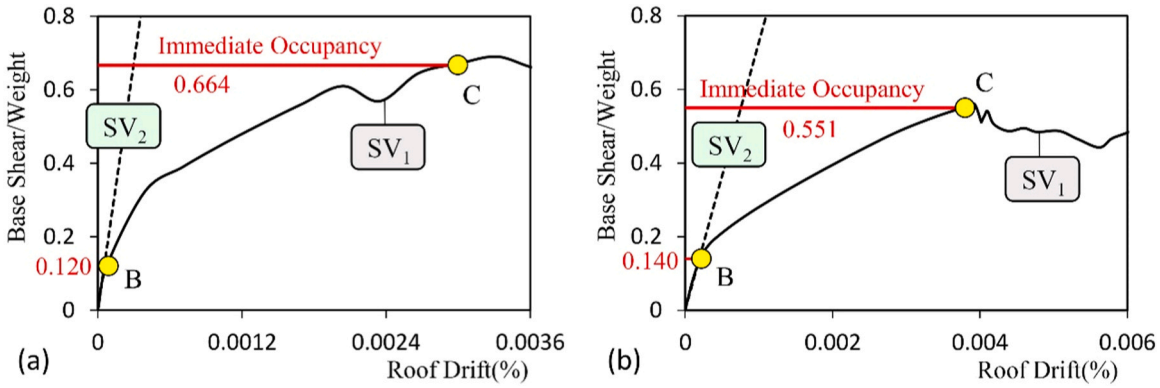


**Fig. 12.** The capacity curves for models with nonlinear shear and linear flexural behavior (a) 5-story building (b) 10-story building.

determined based on the combination of modes of vibration, with the vibration modes contributing up to 90% of the mass participation along the analysis direction (y-axis). The mass center of the roof is considered the control point for analysis. The base shear variations (V(kN)) with respect to control point displacement (Δ(cm)) constitute the capacity curve of the structure and is the primary outcome of the pushover analysis.

For $SM_1$ and $SM_2$ models, the capacity curves are derived as shown in Fig. 11. According to the modeling approach described in Subsection 4.1, the point of separation of these curves is the initiation point of vertical bar yielding in the walls (point A). It should be noted that in this study, the displacement and base shear responses have been normalized to the overall building height (H(cm)) and total seismic weight (W(kN)), respectively. The yielding of longitudinal bars (in tension or compression) corresponds to the initiation of the flexural yielding of the section. As seen in this figure, the capacity curve of the buildings experiences a drop from point A onwards. This phenomenon can be attributed to significant growth of plastic joint rotation due to the yielding of bars. Investigations indicate that at the point of vertical bar yielding, the base shear of the system exceeds 60% of the total seismic weight of the building (72.8% and 61.5% for 5 and 10-story buildings, respectively).

For $SV_1$ and $SV_2$ models, the capacity curves are depicted in Fig. 12. Based on the modeling approach described in Section 4.2, the point of curve separation (point B) marks the initiation of nonlinear behavior due to shear yielding. It is observed that the nonlinear behavior of the system under shear loading begins for base shear less than 15% of the total seismic weight (12.4% and 14.5% for 5 and 10-story buildings, respectively). The base shear corresponding to the immediate occupancy (IO) performance level of the walls in 5 and 10-story buildings is 66.4% and 55.1% of the total seismic weight, respectively (point C). By comparing points A and B, it becomes evident that the base shear corresponding to vertical bar yielding is several times larger than the base shear corresponding to the initiation of nonlinear shear behavior (6.1 and 4.4 times larger for 5 and 10-story buildings, respectively).

Comparing points A and C reveals that before the yielding of vertical bars, based on the local wall shear failure criterion, some walls have reached the IO performance level.

The base shear corresponding to vertical bar yielding is 10% larger than the base shear corresponding to the IO performance level for nonlinear shear behavior. Considering that both concrete and horizontal bars contribute effectively to the expected shear capacity ($V_{CE}$) of the section, it is evident that the yielding of horizontal bars and the initiation of nonlinear shear behavior in the system occur faster.

**Table 2**
The primary components of the original earthquakes used in the process of generating the artificial ground motion records.

| No. | Earthquake& Year | Station | $M_w$ | $R^a$ (km) | PGA (g) |
|---|---|---|---|---|---|
| 1 | Cape Mendocino (US), 1992 | Eureka – Myrtle & West | 7.01 | 44.60 | 0.18 |
| 2 | Cape Mendocino (US), 1992 | Fortuna – Fortuna Blvd | 7.01 | 23.60 | 0.12 |
| 3 | Landers (US), 1992 | Barstow | 7.28 | 36.10 | 0.14 |
| 4 | Northridge (US), 1994 | Lake Hughes #4B - Camp Mend | 6.69 | 32.30 | 0.10 |
| 5 | Northridge (US), 1994 | Hollywood – Willoughby Ave | 6.69 | 25.70 | 0.25 |
| 6 | Northridge (US), 1994 | Big Tujunga, Angeles Nat F | 6.69 | 24.00 | 0.25 |
| 7 | San Fernando (US), 1971 | Pasadena – CIT Athenaeum | 6.61 | 31.70 | 0.11 |

[a] Closest Distance to Fault Rupture

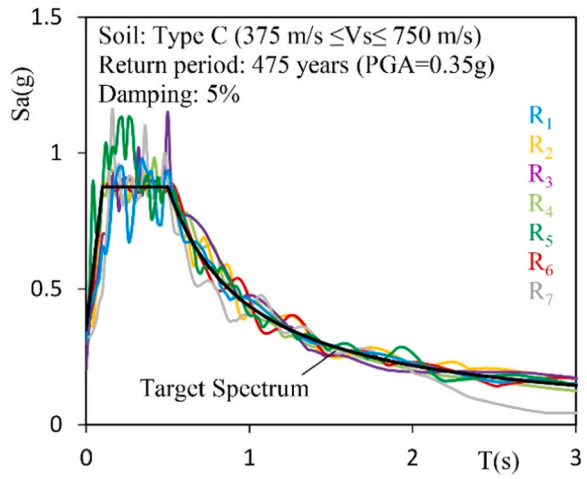


**Fig. 13.** comparison of the spectra of the generated artificial records and the site demand spectrum.

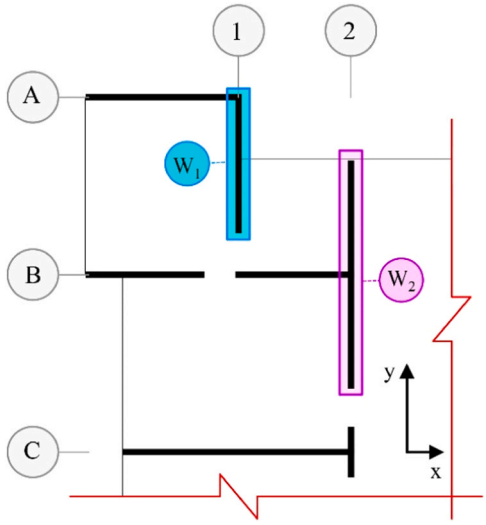


**Fig. 14.** Locations of the examined walls on the plan.

### 5.2. Time-history analysis

Evaluations presented in Subsection 5.1 indicate predominant shear behavior in the system. In this section, the accuracy of the results is assessed through time history analysis.

The design-basis hazard level (475-year return period with a maximum acceleration of 0.35 g) serves as the basis for evaluation. To align the utilized earthquakes as closely as possible with the design spectrum, artificial accelerograms have been generated. The process of producing these artificial records was conducted using the SeismoMatch software [29], based on modifying the original acceleration records.

The primary component of the earthquake's records presented in Table 2, was used for this purpose. The earthquakes are of far-field type and were selected from the PEER website's database [30], considering the site-specific soil conditions (shear wave velocity between 375 to 750 m/s). As depicted in Fig. 13, a desirable correlation can be observed between the peak ground accelerations of the generated artificial records and the target earthquake. Hence, by employing these artificial records in the analysis process, it can be claimed that the models have been evaluated under the target earthquake.

After performing structural analysis, the force and deformation responses in the 3-meter and 5-meter walls located in Plan Axes 1 and 2 (abbreviated as W1 and W2, respectively) have been considered as the evaluation criteria (Fig. 14).

In each time history analysis, for each wall, bending moment ($M_u$) and axial force ($P_u$) at a specific time from the analysis are extracted (Fig. 15(a)). The capacity analysis of the wall section is performed using the interaction curve of the bending moment and axial force (Fig. 15(b)). A combination of these obtained responses, which results in the worst-case scenario, has been considered as the criterion.

For the buildings, the distribution of critical axial force and bending moment demands in the height of structures have been extracted according to Figs. 16 and 17.

In order to develop the interaction curve of bending moment and axial force for the intersecting walls, the effective width of the wall is also considered in the calculations. However, in the present study, to reach the worst possible conditions in estimating the flexural-axial capacity of the section, the effective width of the intersecting walls is disregarded. The geometric properties of the section and the arrangement of reinforcing bars in walls $W_1$ and $W_2$ are described in Table 3 according to Fig. 18(a). As explained earlier, in the relevant calculations, no reduction factor for material strength has been considered. Finally, the interaction bending-axial force for the walls is extracted according to Fig. 18(b) and Fig. 18(c).

According to ASCE recommendations, the axial force in walls and elements controlled by shear should not exceed the limit value $P_0$ as defined in Eq.2 [13]. Otherwise, the element will be classified as force-controlled. The initial step in evaluations involves comparing the axial force demand in the wall with the calculated value from Eq.2:

$$P_0 = 0.15 f_c A_g \tag{2}$$

In this equation, $f_c$ and $A_g$, which represent the characteristic compressive strength of concrete and the gross cross-sectional area of the wall, respectively ($A_g = t_w \quad L_w$).

For a known the axial force demand at the critical section of the wall ($P_u$), the value of the corresponding flexural moment ($M_n$) is determined from the capacity curve.

Obviously, the obtained value signifies the allowable flexural capacity of the wall when the axial force value ($P_u$) is applied. Comparing the flexural demand at the critical section of the wall ($M_u$) with its flexural capacity is the final step of evaluation.

The values of demand and capacity for walls in the case of buildings subjected to records number 1 ($R_1$) are extracted as presented in Tables 4 and 5. For better understanding, the critical values of flexural demand and axial force are compared to the flexural-axial capacity of the wall, as shown in Figs. 19 and 20.

It can be observed that the demand lies within the safe range of the capacity curve. The flexural capacity of the section satisfies the flexural demand ($M_u < M_n$), and the wall has a high safety margin against flexural-axial failure. Additionally, the axial force level is always lower than the ultimate value ($P_u < P_0$). Similar results have been observed for other accelerograms as well (Figs. 21 and 22).

Evaluation of Fig. 21 reveals that the ratio of axial force demand to the ultimate axial force is consistently less than one (maximum ratios of 0.35 and 0.92 for 5-story and 10-story buildings, respectively). Consequently, shear failure of the walls under shear forces can be considered as deformation-control. In the design/performance analysis of the tunnel-form concrete system, it is evident that increasing the wall thickness or using higher strength concrete are the strategies to mitigate the effects of axial forces and ensure sufficient shear deformation capacity of the walls (refer to Eq.2 again).

In Fig. 22, it is observed that in the case of bending moments, the ratio of demand to capacity is always less than 0.75 (0.72 for the 5-story building and 0.57 for the 10-story building). Thus, under the design-basis hazard level, the walls still possess substantial flexural capacity and are far from failure under the existing demand.

The distribution of maximum shear strain of walls in the height of

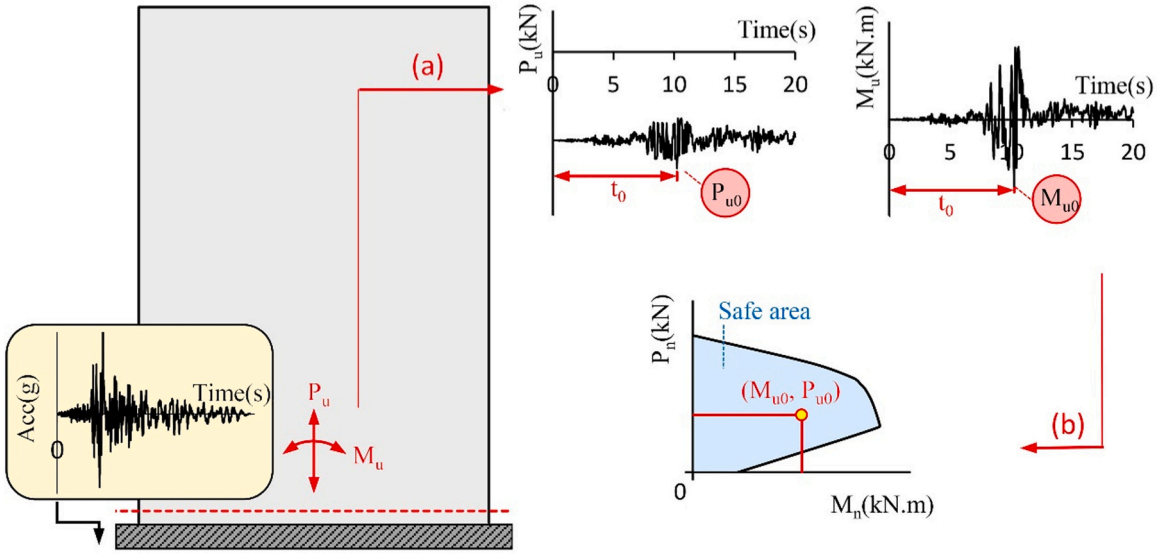


**Fig. 15.** Time history analysis of the shear wall system (a) demand in the critical section of the wall (b) comparison of the demand with the flexural-axial capacity of the wall.

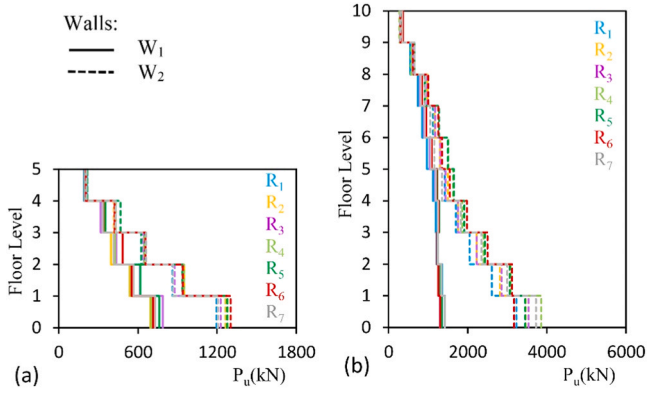


**Fig. 16.** Distribution of the critical axial force demand of the walls in the height of models (a) 5-story building (b) 10-story building.

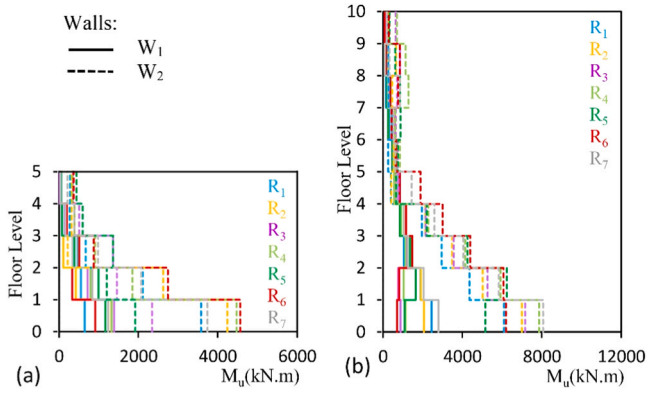


**Fig. 17.** Distribution of the bending moment corresponding to the critical axial force demand of the walls in the height of models (a) 5-story building (b) 10-story building.

structures under the design-basis earthquake is illustrated in Fig. 23. In this figure, the parameter $\gamma_0$ represents the shear strain at the onset of nonlinear shear behavior in walls. According to the shear behavior curve in Fig. 10, this strain corresponds to the initial change in slope of the shear behavior curve and its numerical value can be easily calculated. Fig. 23 indicates that under the design-basis seismic intensity, shear strains exceeding 13 times $\gamma_0$ are experienced (13.76 and 14.79 times $\gamma_0$ for 5-story and 10-story buildings, respectively).

Although the initiation of nonlinear behavior in walls due to shear actions is certain, the level of damage in them remains limited and they have not yet reached the IO performance level (corresponding to a shear strain of 0.004 radians) [13].

As previously mentioned, the parameter α is a geometric criterion predicting the failure mode of walls, and for shear-wall systems, its value should be less than 2 (1.5 according to ASCE [13]) [16].

The results of this section confirm the shear failure of the walls under shear forces in the system. This is despite the fact that for both types of walls, $W_1$ and $W_2$, in the studied buildings, the parameter $\alpha$ has consistently been estimated to be greater than 2 (1.5 according to ASCE [13]) (see Table 6).

According to the design code recommendations, it was expected that in both tunnel-form buildings, the walls would exhibit ductile behavior, and the dominant failure mode in them would be flexural. It can be observed that the geometric criterion of the design code for estimating the failure mode of walls is not suitable for the tunnel-form system and provide inaccurate predictions.

According to the results of this section, the modeling process of the tunnel-form system can be performed solely by considering the nonlinear shear behavior of elements, disregarding steel and concrete fibers.

In other words, a fiber model of the system without considering nonlinear shear behavior, despite imposing high computational effort [31], will lead to incorrect results.

**Table 3**
The reinforcing bars used in the walls (values given in centimeters).

| Buildings | Walls | $t_w$ | $L_w$ | $L_c$ | $L_b$ | $\varphi_b$ | $\varphi_w$ |
|---|---|---|---|---|---|---|---|
| 5-Story (all stories) | $W_1$ | 20 | 300 | 5 | 40 | $\Phi_{12}$ | $\Phi_8$ |
| | $W_2$ | 20 | 500 | 5 | 70 | $\Phi_{12}$ | $\Phi_8$ |
| 10-Story (stories 1 to 4) | $W_1$ | 20 | 300 | 5 | 40 | $\Phi_{18}$ | $\Phi_{12}$ |
| | $W_2$ | 20 | 500 | 5 | 70 | $\Phi_{18}$ | $\Phi_{12}$ |
| 10-Story (stories 1 to 4) | $W_1$ | 20 | 300 | 5 | 40 | $\Phi_{12}$ | $\Phi_8$ |
| | $W_2$ | 20 | 500 | 5 | 70 | $\Phi_{12}$ | $\Phi_8$ |

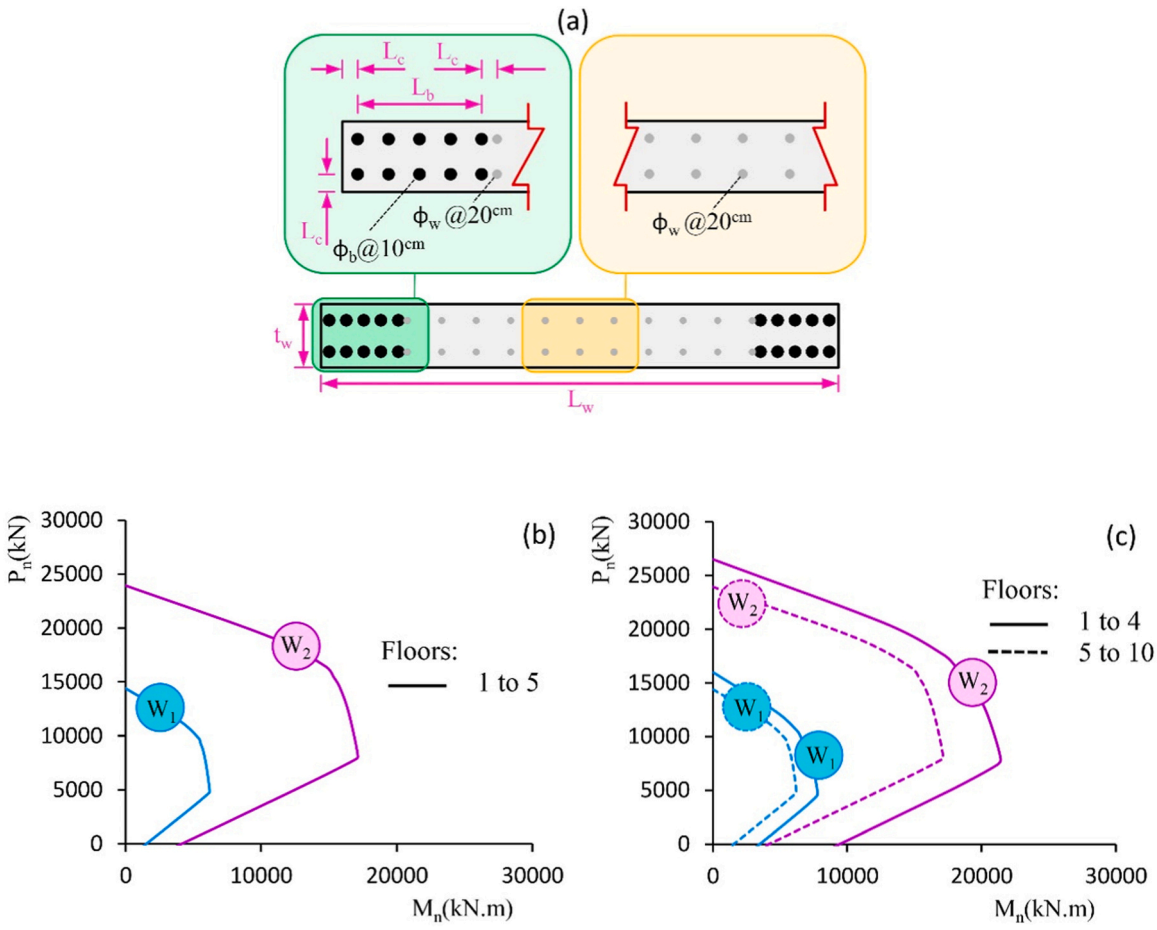


**Fig. 18.** The shear wall sections and their capacity (a) introduction of geometric parameters and section reinforcement details (b) Flexural-axial capacity of walls in the 5-story building (c) Flexural-axial capacity of walls in the 10-story building.

**Table 4**
Demand and Capacity of Wall $W_1$ under accelerogram $R_1$.

| Story no. | $P_u$ (kN) | | $M_u$ (kN.m) | | $P_0$ (kN) | | $M_n$ (kN.m) | |
|---|---|---|---|---|---|---|---|---|
| | 5-Story | 10-Story | 5-Story | 10-Story | 5-Story | 10-Story | 5-Story | 10-Story |
| 1 | 716.0 | 1601.4 | 649.1 | 2451.0 | 2250.0 | 2250.0 | 2300.0 | 4900.0 |
| 2 | 559.2 | 1350.0 | 549.0 | 1892.0 | 2250.0 | 2250.0 | 2100.0 | 4850.0 |
| 3 | 416.7 | 1211.0 | 471.0 | 1063.0 | 2250.0 | 2250.0 | 2000.0 | 4720.0 |
| 4 | 325.6 | 1193.0 | 156.0 | 855.3 | 2250.0 | 2250.0 | 1918.0 | 4700.0 |
| 5 | 189.5 | 1117.0 | 18.0 | 564.0 | 2250.0 | 2250.0 | 1792.0 | 2660.0 |
| 6 | - | 975.2 | - | 468.0 | - | 2250.0 | - | 2552.0 |
| 7 | - | 848.3 | - | 353.0 | - | 2250.0 | - | 2430.0 |
| 8 | - | 736.8 | - | 163.0 | - | 2250.0 | - | 2300.0 |
| 9 | - | 548.7 | - | 147.0 | - | 2250.0 | - | 2100.0 |
| 10 | - | 286.2 | - | 92.6 | - | 2250.0 | - | 1850.0 |

## 6. Energy dissipation in the dominant failure mode

In the technical literature, sometimes brittle failure modes are reported. Due to the minimal energy dissipation in brittle failures, such failure modes should be generally avoided by considering suitable design detailing in the structural design process. Based on the structural analysis results in Section 5, for the tunnel-form concrete system, the dominant shear failure mode in the main lateral load-carrying components (walls and coupling beams) is highly probable. In such conditions, within the range of nonlinear shear behavior, the contribution of the elements in absorbing and dissipating energy is not clear.

According to Fig. 24, the energy balance diagram ($E_T$) for a ground motion excitation includes energy dissipated due to the nonlinear behavior of elements ($E_1$), modal damping ($E_2$), strain energy ($E_3$), and kinetic energy ($E_4$).

The primary elements of the lateral load-carrying system dissipate a percentage of the total earthquake input energy ($E_T$) as they enter the nonlinear behavior range. For tunnel-form buildings, this energy is defined as the sum of the energy dissipated in the coupling beams and walls. Due to plan symmetry, it is sufficient to investigate the energy absorbed by the walls and coupling beams located in axes 1 and 2 (Fig. 25).

Considering $E_1$ plots in Fig. 24, more than 70% of the total earthquake input energy due to accelerogram $R_1$ is consumed by the structural elements (74.22% for the 5-story building and 74.82% for the 10-story building). According to Table 7, this conclusion holds true for

**Table 5**
Demand and Capacity of Wall $W_2$ under accelerogram $R_1$.

| Story no. | $P_u$ (kN) | | $M_u$ (kN.m) | | $P_0$ (kN) | | $M_n$ (kN.m) | |
|---|---|---|---|---|---|---|---|---|
| | 5-Story | 10-Story | 5-Story | 10-Story | 5-Story | 10-Story | 5-Story | 10-Story |
| 1 | 1196.0 | 3227.0 | 3578.0 | 6098.0 | 3750.0 | 3750.0 | 6200.0 | 14800.0 |
| 2 | 860.3 | 2606.0 | 2110.0 | 4352.0 | 3750.0 | 3750.0 | 5600.0 | 13900.0 |
| 3 | 645.7 | 2042.0 | 673.0 | 2954.0 | 3750.0 | 3750.0 | 5300.0 | 13000.0 |
| 4 | 429.1 | 1702.0 | 273.0 | 1952.0 | 3750.0 | 3750.0 | 5000.0 | 12300.0 |
| 5 | 211.9 | 1421.0 | 279.0 | 405.0 | 3750.0 | 3750.0 | 4500.0 | 6500.0 |
| 6 | - | 1306.0 | - | 260.0 | - | 3750.0 | - | 6400.0 |
| 7 | - | 1128.0 | - | 466.6 | - | 3750.0 | - | 6200.0 |
| 8 | - | 955.8.0 | - | 279.0 | - | 3750.0 | - | 6000.0 |
| 9 | - | 645.7 | - | 266.0 | - | 3750.0 | - | 5300.0 |
| 10 | - | 292.5 | - | 250.0 | - | 3750.0 | - | 4800.0 |

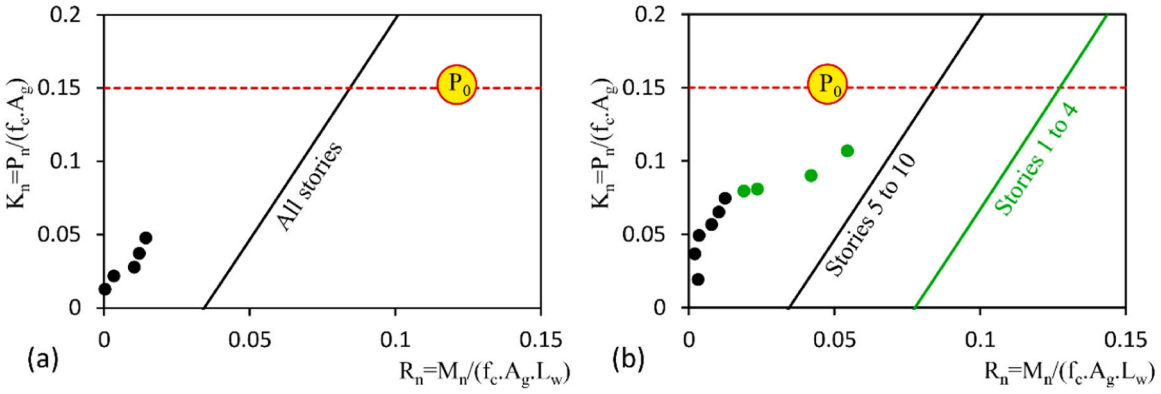


**Fig. 19.** Comparison of demand and capacity of wall $W_1$ in (a) 5-story and (b) 10-story buildings.

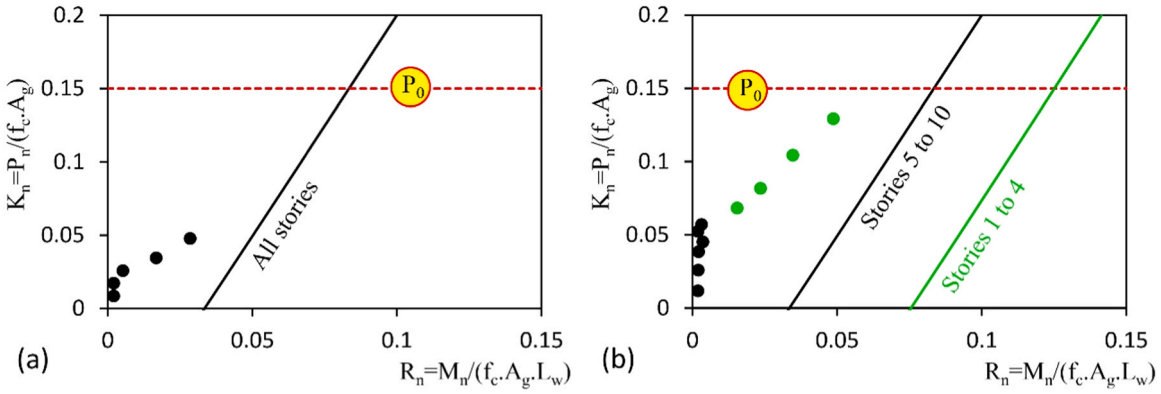


**Fig. 20.** Comparison of demand and capacity of wall $W_2$ in (a) 5-story and (b) 10-story buildings.

other accelerograms as well.

According to Fig. 25, from the total energy dissipated due to nonlinear behavior in the members (represented as T), the share of walls and coupling beams located in axis 1 (and axis 4) is close to 14%, and the share of elements located in axis 2 (and axis 3) is close to 35%. However, considering the contribution of each axis to the overall lateral stiffness of the building, this observation appears reasonable. For other ground motion records as well, the results are quite similar (Table 8).

it is observed that under the design-level seismic demand, the contribution of nonlinear shear behavior of elements to the dissipation of seismic input energy is significant (minimum of 71.45% for the 5-story building and 70.35% for the 10-story building). Accordingly, the shear actions in the elements of the system are deformation-control and their failure under shear forces is deemed the desirable failure mode.

## 7. Conclusion

The present study aimed to determine the probable failure mode of walls in the tunnel-form concrete system. The modeling process of the studied structures is based on the fiber plasticity model, allowing for the occurrence of flexural and shear failures. In order to determine the contributions of shear and flexural actions in the failure of walls, two distinct approaches were adopted. In the first approach, considering linear behavior in shear, the possibility of longitudinal rebar yielding due to flexural moments is investigated. In the second approach, linear behavior is assumed for steel and concrete fibers, and the performance of walls under shear actions is studied. In the range of studied models and adopted assumptions, the following conclusions are drawn from the performed analyses:

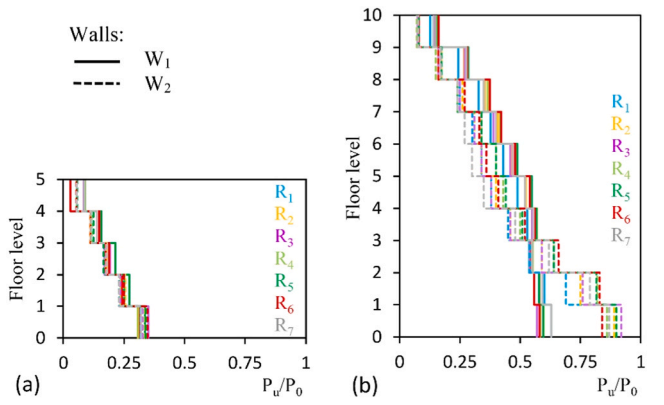


**Fig. 21.** Ratio of critical axial force demand to ultimate axial force in walls of (a) 5-story and (b) 10-story buildings.

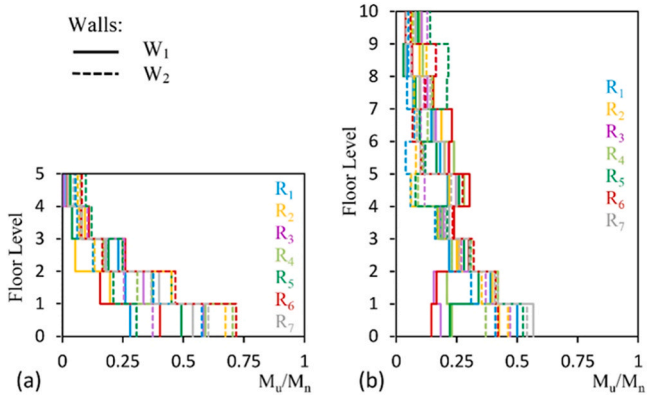


**Fig. 22.** Ratio of bending moment demand to wall flexural capacity in (a) 5-story and (b) 10-story buildings.

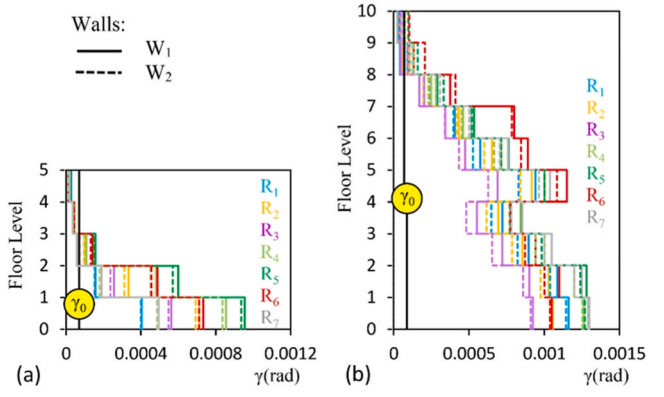


**Fig. 23.** Distribution of maximum shear strain of walls in the height of structures and the limit state corresponding to the onset of nonlinear shear behavior in models: (a) 5- story and (b) 10-story buildings.

**Table 6**
Calculation of geometric parameter α for walls $W_1$ and $W_2$.

| | 5-Storey building | | 10-Storey building | |
|---|---|---|---|---|
| Walls | $W_1$ | $W_2$ | $W_1$ | $W_2$ |
| α | 5 | 3 | 10 | 6 |

1. In the pushover analysis, the base shear corresponding to the flexural failure of walls (the limit state of vertical bar yielding) was calculated to be several times larger than the base shear corresponding to the initiation of nonlinear behavior under shear loading (6.1 and 4.4 times larger for the 5 and 10-story buildings, respectively). Moreover, this base shear value was estimated to be 10% larger than the base shear corresponding to the shear failure of walls (limit state of IO performance level). Based on these results, shear failure mode prevails over flexural failure mode in the walls.
2. Considering nonlinear shear behavior, in the time history analysis under the design earthquake, the shear strain in the walls was calculated to be more than 13 times larger than the shear strain corresponding to the initiation of nonlinear shear behavior due to shear actions. At this intensity level, for critical combinations of axial force demand and bending moments, the wall sections provided sufficient capacity. The maximum ratio of the required flexural demand in walls to the allowable flexural capacity of the section was less than 0.75. In this analysis, the accuracy of the assumptions of deformation-control shear forces and force-control interaction of axial force and bending moments for the tunnel-form concrete walls was confirmed.
3. In the tunnel-form concrete system, under the design earthquake, more than 70% of the input energy is consumed by the nonlinear shear behavior of elements. The results indicate that the failure of elements under shear actions is sufficiently desirable and energy-absorbing.
4. The existing geometric criterion for categorizing shear wall behavior based on the height-to-length ratio (α) is not applicable to the tunnel-form concrete buildings. In the studied buildings, this parameter was calculated to be greater than 2, but contrary to expectations, shear failure mode prevailed in the walls.

In this study, the failure mode of tunnel-form walls has been assessed numerically on full scale numerical models. Modeling and performance evaluation of the system were carried out based on ASCE Standard [13]. In the similar studies, patterns of crack distribution in elements, the precise location and shape of concrete failure, and yielding in bars are not precisely determined. Nevertheless, determining the failure mode and investigating these aspects through detailed finite element analyses (at the micro scale) and laboratory tests on models with real scales should be further investigated in the future research.

## Author statement

We have revised the manuscript entitled "*Numerical Analysis of Potential Failure Modes in Shear Walls of the Tunnel Form Concrete System: Performance-Based Approach*" authored by "Vahid Mohsenian and Luigi DiSarno" based on the reviewers' comments. We would like to re-submit the manuscript to your prestigious journal of "Engineering Structures".

We valued the comments of the reviewers; their suggestions and comments contributed to improve the (new) manuscript. We acknowledge the positive contributions of the anonymous reviewers.

## CRediT authorship contribution statement

**Di Sarno Luigi:** Conceptualization, Data curation, Methodology, Supervision, Validation, Writing – original draft, Writing – review & editing. **Mohsenian Vahid:** Conceptualization, Data curation, Formal analysis, Investigation, Methodology, Writing – original draft, Writing – review & editing.

## Declaration of Competing Interest

I can declare on behalf of my coauthor that we have no conflicting interests regarding submission of this manuscript to Engineering Structural Journal.

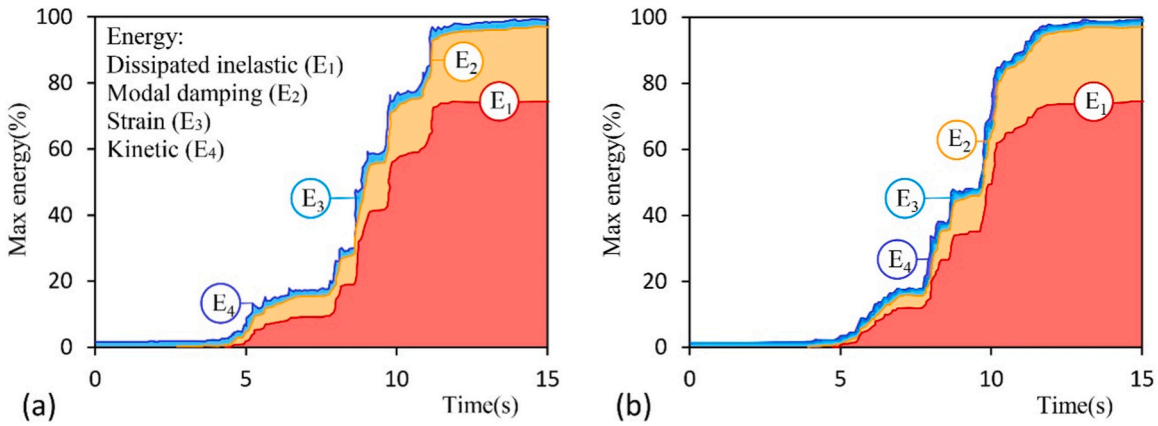


**Fig. 24.** Energy balance under accelerograms $R_1$ (a) 5-Story Building (b) 10-Story Building.

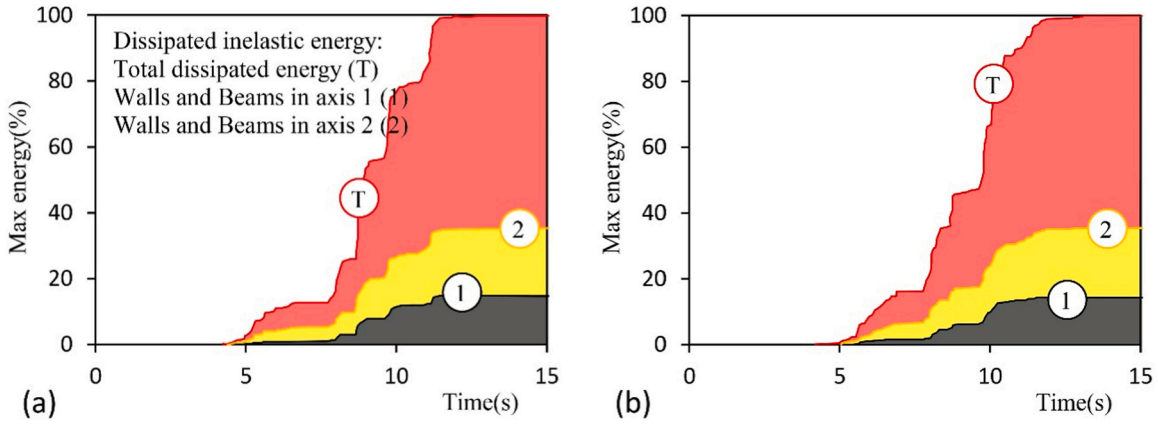


**Fig. 25.** Dissipated Energy in lateral load-carrying members under accelerogram $R_1$ (a) 5-Story Building (b) 10-Story Building.

**Table 7**
Total input energy for mappings ($E_T$) and energy consumed due to nonlinear behavior in buildings ($E_1$).

| Record | $E_T$ ($\times 10^6$ kgf.cm) | | $E_1$ (%) | |
|---|---|---|---|---|
| | 5-Story | 10-Story | 5-Story | 10-Story |
| $R_1$ | 1.41 | 10.79 | 74.22 | 74.82 |
| $R_2$ | 0.57 | 8.59 | 71.45 | 72.79 |
| $R_3$ | 0.73 | 7.11 | 72.79 | 73.51 |
| $R_4$ | 0.89 | 11.24 | 73.63 | 71.61 |
| $R_5$ | 1.59 | 8.49 | 71.72 | 73.03 |
| $R_6$ | 1.31 | 7.81 | 73.14 | 70.35 |
| $R_7$ | 1.02 | 7.13 | 72.32 | 72.43 |

**Table 8**
The share of elements located in axes 1 and 2 of the plan ($E_{D1}$ and $E_{D2}$) from the total energy absorbed and consumed due to nonlinear behavior in the members (T).

| Record | $E_{D1}$ (Axes 1&4:%) | | $E_{D2}$ (Axes 2&3:%) | |
|---|---|---|---|---|
| | 5-Story | 10-Story | 5-Story | 10-Story |
| $R_1$ | 14.68 | 14.21 | 35.08 | 35.44 |
| $R_2$ | 15.39 | 14.32 | 34.61 | 35.32 |
| $R_3$ | 15.87 | 15.51 | 34.01 | 34.25 |
| $R_4$ | 16.35 | 14.68 | 33.77 | 34.96 |
| $R_5$ | 14.20 | 15.50 | 35.68 | 34.01 |
| $R_6$ | 15.16 | 13.48 | 35.08 | 36.28 |
| $R_7$ | 14.92 | 14.68 | 35.20 | 34.84 |

## Data availability

Data will be made available on request.

## Acknowledgments

The authors express their gratitude to Dr. Egemen Sönmez for sharing the images obtained from the earthquake experiences and damages of the 2023 Turkey earthquakes.

## References

[1] Mohsenian V, Filizadeh R, Nikkhoo A, Hajirasouliha I. Multi-level response modification factors for performance-based seismic design of tunnel-form building structures. J Earthq Eng 2023 (In press.).
[2] Mohsenian V, Gharaei-Moghaddam N, Hajirasouliha I. Seismic performance assessment of tunnel form concrete structures under earthquake sequences using endurance time analysis. J Build Eng 2021;40(2021):102327.
[3] Balkaya C, Kalkan E. Seismic vulnerability, behavior and design of tunnel form building structures. Eng Struct 2004;26(14):2081–99.
[4] Aksu Ozkul T, Kurtbeyoglu A, Borekci M, Zengin B, Kocak A. Effect of shear wall on seismic performance of RC frame buildings. Eng Fail Anal 2019;100:60–75.
[5] Balkaya C, Kalkan E. Nonlinear seismic response evaluation of tunnel form building structures. Comput Struct 2003;81(3):153–65.
[6] Yuksel SB, Kalkan E. Behavior of tunnel form buildings under quasi-static cyclic lateral loading. Struct Eng Mech 2007;27(1):99–115.
[7] Kalkan E, Yuksel SB. Pros and cons of multistory RC tunnel-form (box-type) buildings. Struct Des Tall Spec Build 2007;17(3):601–17.
[8] Brunesi E, Peloso S, Pinho R, Nascimbene R. Cyclic testing and analysis of a full-scale cost-in-place reinforced concrete wall-slab-wall structure. Bull Earthq Eng 2018;16:4761–96.
[9] Tavafoghi A, Eshghi S. Evaluation of behavior factor of tunnel-form concrete building structures using applied technology council 63 methodology. Struct Des Tall Spec Build 2013;22(8):615–34.

[10] Fadallah R, Elbayomy M, Ghith H, Salem H. Experimental investigation of small-scale shear walls under lateral loads. J Eng Appl Sci 2022;69(85):1–19.
[11] Jim L, Zhang B, Chen F, Yu W, Lei Y, Miao L, et al. Numerical investigations on the strain-rate-dependent mechanical behavior and size effect of RC shear walls. Int Impact Eng 2022;167:104279.
[12] IBHRC (2007). Approved technologies indirection of sub-note 2–6, paragraph "D", Note 6, "A step in direction of building industrialization", first edition, Building and Housing Research Center Press, pages 21 and 22.
[13] ASCE/SEI 41–17. 2017. Seismic Evaluation and Retrofit of Existing Buildings. Reston, VA: American Society of Civil Engineers.
[14] Morius M. Seismic behaviour of reinforced concrete shear walls with regular and staged openings after the strong earthquakes between 2009 and 2011. Eng Fail Anal 2013;34:537–65.
[15] Miao L, Jin L, Li D, Du X, Zhang B. Effect of shear-span ratio and vertical reinforcement ratio on the failure of geometrical-similar RC shear walls. Eng Fail Anal 2022;139:106407.
[16] American Concrete Institute, 2019. Building Code Requirements for Structural Concrete (ACI 318–19). Farmington Hills, MI: ACI.
[17] ASCE, 2022, Minimum Design Loads and Associated Criteria for Buildings and Other Structures, ASCE/SEI 7–22, American Society of Civil Engineers, Reston, Virginia.
[18] Permanent Committee for Revising the Standard 2800. (2014), Iranian Code of Practice for Seismic Resistant Design of Buildings, 4th Edition, Building and Housing Research Center, Tehran, Iran.
[19] CSI), (2015). Structural and Earthquake Engineering Software, ETABS, Extended Three Dimensional Analysis of Building Systems Nonlinear Version 15.2.2, Berkeley, CA, USA.
[20] Balkaya C, Kalkan E. Estimation of fundamental periods of shear-wall dominant building structures. Earthq Eng Struct Dyn 2003;32(7):985–98.
[21] CSI), 2016. Structural and Earthquake Engineering Software, PERFORM-3D Nonlinear Analysis and Performance Assessment for 3D Structures, Version 6.0.0, Berkeley, CA, USA.
[22] Paulay T, Binney JR. Diagonally Reinforced Coupling Beams of Shear Walls, Shear in Reinforced Concrete, 42. ACI Special Publications,; 1974. p. 579–98.
[23] Zhao ZZ, Kwan AKH, He XG. Nonlinear finite element analysis of deep reinforced concrete coupling beams. Eng Struct 2004;26(1):13–25.
[24] Mosoarca M. Failure analysis of RC shear walls with staggered openings under seismic loads. Eng Fail Anal 2014;41:48–64.
[25] Liu Y, Zhou W. Numerical modeling to predict seismic performance of the post-tensioned self-centering concrete shear walls. Bull Earthq Eng 2022;20(2):1057–86.
[26] Kolozvari K, Kalbasi K, Orakcal K, Wallance J. Three-dimensional shear-flexure interaction for analysis of non-planar reinforced concrete walls. J Build Eng 2021;44(2021):102946.
[27] Menegotto, M. and Pinto, P.E., 1973. Method of analysis for cyclically loaded RC plane frames including changes in geometry and non-elastic behavior of elements under combined normal force and bending. In Proc. of IABSE Symposium on Resistance and Ultimate Deformability of Structures Acted on by Well Defined Repeated Loads, Zurich, Switzerland.
[28] Mander JB, Priestley MJ, Park R. Theoretical stress-strain model for confined concrete. J Struct Eng 1988;114(8):1804–26.
[29] https://seismosoft.com/.
[30] PEER Ground Motion Database, Pacific Earthquake Engineering Research Center, Web Site: https://ngawest2.berkeley.edu/; Accessed: Jan 2021.
[31] Mohsenian V, Nikkhoo A, Hajirasouliha I, Hejazi F. A low computational cost seismic analyses framework for 3D tunnel-form building structures. Adv Struct Eng 2022;0(0):1–15.